World Academy of Science, Engineering and Technology
International Journal of Mechanical and Mechatronics Engineering
Vol:5, No:6, 2011

Study of Heat Transfer in the Poly Ethylene Fluidized Bed Reactor Numerically and Experimentally

Mahdi Hamzehei

Open Science Index, Mechanical and Mechatronics Engineering Vol:5, No:6, 2011 publications.waset.org/6657/pdf

***Abstract*—**In this research, heat transfer of a poly Ethylene fluidized bed reactor without reaction were studied experimentally and computationally at different superficial gas velocities. A multi-fluid Eulerian computational model incorporating the kinetic theory for solid particles was developed and used to simulate the heat conducting gas–solid flows in a fluidized bed configuration. Momentum exchange coefficients were evaluated using the Syamlal–O'Brien drag functions. Temperature distributions of different phases in the reactor were also computed. Good agreement was found between the model predictions and the experimentally obtained data for the bed expansion ratio as well as the qualitative gas–solid flow patterns. The simulation and experimental results showed that the gas temperature decreases as it moves upward in the reactor, while the solid particle temperature increases. Pressure drop and temperature distribution predicted by the simulations were in good agreement with the experimental measurements at superficial gas velocities higher than the minimum fluidization velocity. Also, the predicted time-average local voidage profiles were in reasonable agreement with the experimental results. The study showed that the computational model was capable of predicting the heat transfer and the hydrodynamic behavior of gas-solid fluidized bed flows with reasonable accuracy.

***Keywords*—**Gas-solid flows, fluidized bed, Hydrodynamics, Heat transfer, Turbulence model, CFD

I. Introduction

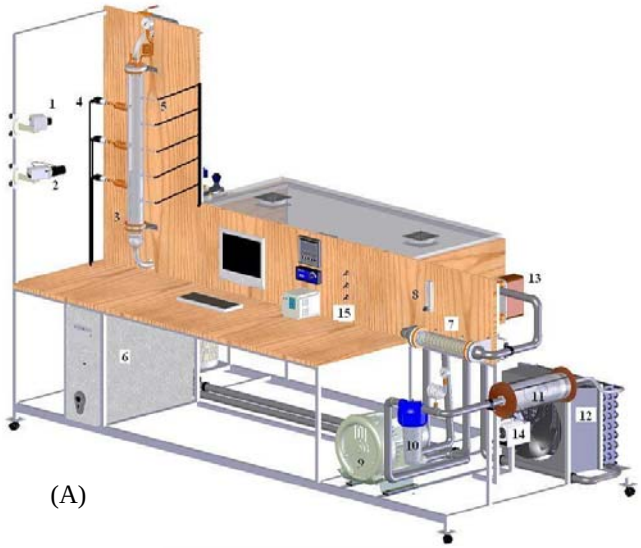
TWO-PHASE flows occur in many industrial and environmental processes. These include pharmaceutical, petrochemical, and mineral industries, energy conversion, gaseous and particulate pollutant transport in the atmosphere, heat exchangers and many other applications. The gas–solid fluidized bed reactor has been used extensively because of its capability to provide effective mixing and highly efficient transport processes. Understanding the hydrodynamics and heat transfer of fluidized bed reactors is essential for their proper design and efficient operation. Gas–solid flows at high concentration in these reactors are quite complex because of the coupling of the turbulent gas flow and fluctuation of particle motion dominated by inter-particle collisions. These complexities lead to considerable difficulties in designing, scaling up and optimizing the operation of these reactors [1-3]. Despite a significant amount of research on fluidized bed reactors, there are considerable uncertainties on their behavior. Part of the confusion is due to the presence of various complex flow regimes and their sensitivities to the operating conditions of these reactors. The fundamental problem encountered in modeling the hydrodynamics of a gas–solid fluidized bed is the strong interaction of the phases with unknown and transient interfaces. As a result, the interaction of the phases is understood only for a limited range of conditions. One additional important complexity is that in many of these industrial processes the gas flow is in a turbulent state of motion [3-6]. Kaneko et al. [7] numerically analyzed temperature behavior of particles and gas in a fluidized bed reactor by applying a discrete element method, where heat transfer from particles to the gas was estimated using Ranz–Marshall equation. CFD simulation of a fluidized bed reactor was also conducted by Rong et al. [8] focusing on the chemical kinetic aspects and taking into account the intra-particle heat and mass transfers, poly-disperse particle distributions, and multiphase fluid dynamics. Gas–solid heat and mass transfer, polymerization chemistry and population dynamic equations were developed and solved in a multi-fluid code (MFIX) in order to describe particle growth. Gobin et al. [9] numerically simulated a fluidized bed using a two-phase flow method. In their study, time-dependent simulations were performed for industrial and pilot reactor operating conditions. Their numerical predictions were in qualitative agreement with the observed behavior in terms of bed height, pressure drop and mean flow regimes. Van Wachem et al. [10,11] verified experimentally their Eulerian-Eulerian gas-solid simulations of bubbling fluidized beds with existing correlations for bubble size or bubble velocity. Chiesa et al. [12] have presented a computational study of the flow behavior of a lab-scale fluidized bed. The results obtained from a 'discrete particle method' (DPM) were qualitatively compared with the results obtained from a multi-fluid computational fluid dynamic (CFD) model. Despite many studies on the modeling and model evaluation of fluidized-bed hydrodynamics, only a few works have been published on the CFD modeling and model validation of combined reactor hydrodynamics and heat transfer. In this study, the heat transfer and hydrodynamics of a two-dimensional non-reactive gas–solid fluidized bed reactor were studied experimentally and computationally. Attention was given to

Mahdi Hamzehei is with Department of Mechanical Engineering, Ahvaz Branch Islamic Azad University, Ahvaz, Iran, (email: mahdi_hamzei@iauahvaz..ac.ir)

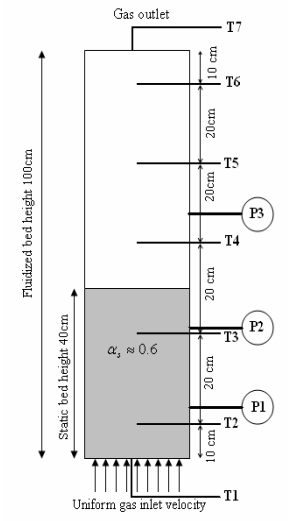
Open Science Index, Mechanical and Mechatronics Engineering Vol:5, No:6, 2011 publications.waset.org/6657/pdf

the influence of gas temperature and gas velocity on gas-solid heat transfer and hydrodynamics. A multi-fluid Eulerian model incorporating the kinetic theory for solid particles with the standard $k-\varepsilon$ turbulence model was applied in order to simulate the gas–solid flow at different superficial gas velocities. It was assumed that inlet gas was hot and the initial solid particle was at ambient temperature. Simulation results were compared with the experimental data for model validation.

II. Experimental Set up



(A)



(B)

Fig. 1 (A) A view of experimental set-up (1- digital camera, 2- digital video recorder, 3- Pyrex reactor, 4- pressure transducers, 5- thermocouples, 6- computer , A/D and DVR cards, 7- electrical heater, 8-rotameter, 9-blower, 10- filter, 11-14- cooling system, 15- controller system), (B) : pressure transducer and thermocouple positions in the fluidized bed reactor

A bench scale experimental setup for studying gas-solid flows and heat transfer was designed and fabricated. The setup consists of a Pyrex cylinder with a height of 100cm and a diameter of 25 cm as shown schematically in Figure 1. The air was injected through a perforated plate with an open area of 0.8 % and an orifice diameter of 2 cm. Under this plate there was a homogenization system to prevent the gas flow from generating asymmetrical effects inside the free board. This distribution belongs to group B in the Geldart classification. Spherical particles with a diameter of 300 μm and a density of 1830 kg/m^3 were fluidized with air at ambient conditions. Typically, the static bed height was 40cm with a solid volume fraction of 0.6. A roots-type blower supplied the fluidizing gas. A pressure-reducing valve was installed to avoid pressure oscillations and achieve a steady gas flow. The airflow rate was measured using a gas flow meter. Initial solid particle temperature was 300K. An electrical heater was used to increase the inlet gas temperature from ambient temperature to 473K. A cooling system was used to decrease the gas temperature that exited from the reactor in order to form a closed cycle. Figure 1 (A) shows a schematic of experimental set-up and its equipments. Pressure fluctuations in the bed were measured by three pressure transducers. The pressure transducers were installed in the fluidized bed column at different heights. Seven thermocouples (Type J) were installed in the center of the reactor to measure the variation of gas temperature at different locations. Also, three thermocouples were used in different positions in the set-up to control the gas temperature in the heat exchanger and cooling system. Fig. 1. (B) shows the locations of the pressure transducers and thermocouples. The pressure probes were used to convert fluctuation pressure signals to out-put voltage values proportional to the pressure. The overall pressure drop and bed expansion were monitored at different superficial gas velocities from 0 to 0.8 m/s. For controlling and monitoring the fluidized bed operation process, A/D, DVR cards and other electronic controllers were applied. A video camera (25 frames per s) and a camera (Canon 5000) were used to photograph the flow regimes and bubble formation through the transparent wall (external photographs) during the experiments. The captured images were analyzed using image processing software.

III. Governing Equation

The governing equations of the gas-solid flow include the conservation of mass, momentum, and energy. The governing equations of solid and gas phases are based on the Eularian-Eularian model. By definition, the volume fractions of the phases must sum to one: $\alpha_g + \alpha_s = 1$

The continuity equation for gas and solid phases in the absence of inter-phase mass transfer are respectively given as

$$\frac{\partial}{\partial t}(\alpha_g \rho_g) + \nabla \cdot (\alpha_g \rho_g \overrightarrow{v_g}) = 0 \quad (1)$$

$$\frac{\partial}{\partial t}(\alpha_s \rho_s) + \nabla \cdot (\alpha_s \rho_s \overrightarrow{v_s}) = 0 \quad (2)$$

The conservation of momentum for the gas and solid phases are described by

$$\frac{\partial}{\partial t}(\alpha_g \rho_g \vec{v}_g) + \nabla.(\alpha_g \rho_g \vec{v}_g \vec{v}_g) = -\alpha_g \nabla p_g + \nabla.\overline{\overline{\tau}}_g + \alpha_g \rho_g \vec{g} + \beta_{gs}(\vec{v}_s - \vec{v}_g) \quad (3)$$

$$\frac{\partial}{\partial t}(\alpha_s \rho_s \vec{v}_s) + \nabla \cdot (\alpha_s \rho_s \vec{v}_s \vec{v}_s) = -\alpha_s \nabla p_g \quad (3)$$

$$-\nabla p_s + \nabla.\overline{\overline{\tau}}_s + \alpha_s \rho_s \vec{g} + \beta_{gs}(\vec{v}_g - \vec{v}_s) \quad (4)$$

Here $\overline{\overline{\tau}}$ is Reynolds stress tensor, g is gravitational constant and $(-\alpha_s \nabla p + \beta_{gs}(\vec{v}_g - \vec{v}_s))$ is an interaction force (drag and buoyancy forces) representing the momentum transfer between gas and solid phases [1, 5, 6].

Several drag models for the gas-solid inter-phase exchange coefficient β_{gs} were reported in the literature. The drag model of Syamlal-O'Brien [13, 14] were used in the present study. The drag model of Syamlal-O'Brien is based on the measurements of the terminal velocities of particles in fluidized or settling beds. The corresponding inter-phase exchange coefficient is expressed as

$$\beta_{gs} = \frac{3}{4}\frac{\alpha_s \alpha_g \rho_g}{\upsilon_{r,s}^2 d_s} C_D\left(\frac{\mathrm{Re}_s}{\upsilon_{r,s}}\right)\left|\vec{\upsilon}_s - \vec{\upsilon}_g\right| \quad (5)$$

$$C_D = \left(0.63 + \frac{4.8}{\sqrt{\mathrm{Re}_s / \nu_{r,s}}}\right)^2 \quad (6)$$

and $\nu_{r,s}$, a terminal velocity correlation, is expressed as

$$\upsilon_{r,s} = 0.5\left(A - 0.06\mathrm{Re}_s + \sqrt{(0.06\mathrm{Re}_s)^2 + 0.12\mathrm{Re}_s(2B - A) + A^2}\right) \quad (7)$$

$$A = \alpha_g^{4.14} \text{ and } B = 0.8\alpha_g^{1.28} \text{ for } \varepsilon_g \le 0.85 \text{ and } B = \alpha_g^{2.65} \text{ for } \alpha_g > 0.85 \quad (8)$$

The granular temperature (Θ) of the solid phase is defined as one-third of the mean square particle velocity fluctuations. It should be emphasized that this is proportional to the granular energy and is given as [13, 14, 20, 21, 23].

$$\frac{3}{2}\frac{\partial}{\partial t}(\rho_s \alpha_s \Theta_s) + \nabla \cdot (\rho_s \alpha_s \vec{v}_s \Theta_s) = (-p_s \overline{\overline{I}} + \overline{\overline{\tau}}_s) : \nabla.\vec{v}_s + \nabla \cdot (k_{\Theta_s} \nabla \Theta_s) - \gamma_{\Theta_s} + \phi_{gs} \quad (9)$$

where $(-p_s \overline{\overline{I}} + \overline{\overline{\tau}}_s) : \nabla.\vec{v}_s$ is the generation of energy by the solid stress tensor, $k_{\Theta_s} \nabla \Theta_s$ is the diffusion flux of granular energy (k_{Θ_s} is the diffusion coefficient), γ_{Θ_s} is the collisional dissipation of energy and ϕ_{gs} is the energy exchange between the gas and solid. The collision dissipation of energy, γ_{Θ_s}, representing the rate of energy dissipation within the solid phase due to inelastic particle collisions that was derived by Lun et al. [16] is given as

$$k_{\Theta_s} = \frac{15 d_s \rho_s \alpha_s \sqrt{\pi \Theta_s}}{4(41 - 33\eta)}\left[1 + \frac{12}{5}\eta^2(4\eta - 3)\alpha_s g_{o,ss} + \frac{16}{15\pi}(41 - 33\eta)\eta\alpha_s g_{o,ss}\right]$$

$$\gamma_{\Theta_s} = \frac{12(1 - e_{ss}^2) g_{o,ss}}{d_s \sqrt{\pi}} \rho_s \alpha_s^2 \Theta_s^{3/2} \quad (10)$$

The transfer of kinetic energy, ϕ_{gs}, due to random fluctuations in particle velocity is expressed as [1]

$$\phi_{gs} = -3\beta_{gs}\Theta_s \quad (11)$$

For granular flows a solids pressure is calculated independently and used for the pressure gradient term, p_s, in the granular-phase momentum equation. Because a Maxwellian velocity distribution is used for the particles, a granular temperature is introduced into the model and appears in the expression for the solid pressure and viscosities. The solid pressure is composed of a kinetic term and a second term due to particle collisions:

$$p_s = \alpha_s \rho_s \Theta_s + 2\rho_s(1 + e_{ss})\alpha_s^2 g_{o,ss}\Theta_s \quad (12)$$

where e_{ss} is the coefficient of restitution for particle collisions, and $g_{o,ss}$ is the radial distribution function.

The solid stress tensor contains shear and bulk viscosities arising from particle momentum exchange due to translation and collision. A frictional component of viscosity can also be included to account for the viscous-plastic transition that occurs when particles of a solid phase reach the maximum solid volume fraction.

The collisional and kinetic parts, and the frictional part, were used to evaluate the solid shear viscosity. That is,

$$\mu_s = \mu_{s,col} + \mu_{s,kin} + \mu_{s,fr} \quad (13)$$

The collisional part of the shear viscosity is modeled as

$$\mu_{s,col} = \frac{4}{5}\alpha_s \rho_s d_s g_{o,ss}(1 + e_{ss})\left(\frac{\Theta_s}{\pi}\right)^{1/2} \quad (14)$$

The kinetic term is expressed in the Syamlal-O'Brien [20, 21] model as :

$$\mu_{s,kin} = \frac{\alpha_s \rho_s d_s \sqrt{\Theta_s \pi}}{6(3 - e_{ss})}\left[1 + \frac{2}{5}(1 + e_{ss})(3e_{ss} - 1)\alpha_s g_{o,ss}\right] \quad (15)$$

The friction stress plays a significant role when the solid-phase volume fraction gets close to the packing limit. For the contribution of the friction stress to the solid shear viscosity the expression suggested by Schaeffer [8] given as

Open Science Index, Mechanical and Mechatronics Engineering Vol:5, No:6, 2011 publications.waset.org/6657/pdf

$$\mu_{s,fr} = \frac{p_s \sin\phi}{2\sqrt{I_{2D}}} \quad (16)$$

is used. Here p_s is the solid pressure, ϕ is the angle of internal friction, and I_{2D} is the second invariant of the deviatoric stress tensor [5, 8, 11]. The solid bulk viscosity accounts for the resistance of the granular particles to compression and expansion. It has the following from Lun et al. [16]:

$$\lambda_s = \frac{4}{3}\alpha_s \rho_s d_s g_{o,ss}(1+e_{ss})\sqrt{\frac{\Theta_s}{\pi}} \quad (17)$$

The diffusion coefficient for granular energy, k_{Θ_s}, is expressed by two different models. The Syamlal- O'Brien model expresses as [20, 21]

(18)

The internal energy balance for the gas phase can be written in terms of the gas temperature as follows:

$$\alpha_g \rho_g Cp_g \left(\frac{\partial T_g}{\partial t} + v_g.\nabla T_g\right) = -H_{gs} \quad (19)$$

The solid heat conductivity includes direct conduction through the fractional contact area and indirect conduction through a wedge of the gas that is trapped between the particles. Since the gas heat conductivity is negligible, the heat diffusion term has been ignored [11].

The thermal energy balance for the solid phases is given by

$$\alpha_s \rho_s Cp_s \left(\frac{\partial T_s}{\partial t} + v_s.\nabla T_s\right) = \nabla.\alpha_s K_s \nabla T_s + H_{gs} \quad (20)$$

The heat transfer between the gas and the solid is a function of the temperature difference between the gas and solid phases:

$$H_{gs} = -\gamma^0{}_{gs}\left(T_s - T_g\right) \quad (21)$$

The heat transfer coefficient is related to the particle Nusselt number using the following equation:

$$\gamma^0_{gs} = \frac{6k'_g \varepsilon_s Nu_s}{d_s^2} \quad (22)$$

Here k'_g is the thermal conductivity of the gas phase and Nu_s is Nusselt number of solid phase.

A. Initial and boundary conditions

The initial values of the variables for all the fields $(\alpha_g, \alpha_s, v_g, v_s)$ are specified for the entire computational domain. Initially, solid particle velocity was set at zero (in minimum fluidization), and gas velocity was assumed to have the same value everywhere in the bed. At the inlet, all velocities and volume fraction of all phases were specified. Outlet boundary condition was out flow and was assumed to be a fully developed flow. The other variables were subject to the Newmann boundary condition. The gas tangential normal velocities on the wall were set to zero (no slip condition). The normal velocity of the particles was also set at zero. The following boundary condition was applied for the tangential velocity of particles at the wall [28-35] and the general boundary condition for granular temperature at the wall takes the form

$$\vec{v}_{s,w} = -\frac{6\mu_s \alpha_{s,\max}}{\sqrt{3}\pi\rho_s \alpha_s g_{o,ss}\sqrt{\Theta_s}}\frac{\partial \vec{v}_{s,w}}{\partial n} \quad (23)$$

$$\Theta_{s,w} = -\frac{k_s \Theta_s}{e_{ss,w}}\frac{\partial \Theta_{s,w}}{\partial n} + \frac{\sqrt{3}\pi\rho_s \alpha_s v_s^2 g_o \Theta_s^{3/2}}{6\alpha_{s,\max} e_{ss,w}} \quad (24)$$

Here $\vec{v}_{s,w}$ is the particle slip velocity, $e_{ss,w}$ is the restitution coefficient at the wall, and $\alpha_{s,\max}$ is the volume fraction for the particles at maximum packing [11, 15, 28]. The boundary conditions for the energy equation are set such that the walls are adiabatic. Initial solid particles temperature is 300K and the inlet gas temperature is 473K.

B. Model solution procedure

Two-dimensional (2D) simulations of the fluidized bed with heat transfer under steady conditions were performed and the results are described in this section. The Eulerian multiphase model described earlier was used for the analysis. The 2D computational domain was discretized using 8600 rectangular cells. Typically, a time step of 0.001s with 20 iterations per time step was also used. This number of iterations was found to be adequate to achieve convergence for the majority of time steps. Table 1 shows values of model parameters that were used in the simulations. The discretized governing equations were solved by the finite volume method employing the Semi Implicit Method for the Pressure Linked Equations (SIMPLE) algorithm that was developed by Patankar and Spalding [18] for multiphase flow using the Partial Elimination Algorithm (PEA). Several research groups have used extensions of the SIMPLE method, which appears to be the method of choice in commercial CFD codes [6- 9].

TABLE I
VALUES OF PARAMETERS USED IN THE SIMULATIONS AND EXPERIMENTS

Symbol	Description	Value	Comment or reference
ρ_s	Solids density	2130 kg/m^3	Uniform distribution
ρ_g	Gas density	1.189 kg/m^3	Air at ambient conditions
d_s	Mean particle diameter	300 μm	(Geldart B type)Uniform distribution
e_{ss}	Coefficient of restitution	0.9	Fixed value
$\alpha_{\max}$	Maximum solids packing	0.61	Syamlal et al. [13, 14]
ϕ	Angle of internal friction	25^o	Johnson and Jackson [21]
D_t	Column diameter	25 cm	Fixed value

Open Science Index, Mechanical and Mechatronics Engineering Vol:5, No:6, 2011 publications.waset.org/6657/pdf

H_1	Fluidized bed height	100 cm	Fixed value
H_0	Initial static bed height	40 cm	Fixed value
	Initial temperature of solids	300 K	Fixed value
	Inlet gas temperature	473 K	Fixed value
V_g	Superficial gas velocity	0- 80 cm/s	A range was used
	Inlet boundary conditions	Velocity	Superficial gas velocity
	Outlet boundary conditions	Out flow	Fully developed flow

IV. Results and Discussion

Simulation results were compared with the experimental data in order to validate the model. Figure 2 compares the simulated time-averaged bed pressure drops, (P1-P2) and (P1-P3), against the superficial gas velocity with the experimental data. The Syamlal–O'Brien drag expression was used in these simulations. The locations of pressure transducers (P1, P2, P3) were shown in Fig. 1 (B). The simulation and experimental results show good agreement at velocities above $V_{mf.}$. For $V < V_{mf.}$ the solid is not fluidized, and the bed dynamic is dominated by inter-particle frictional forces, which is not considered by the multi-fluid models used. Fig. 2 shows that with increasing gas velocity, initially the pressure drops (P1-P2 and P1-P3) increase, but the rate of increase for (P1-P3) is larger than that for (P1-P2). For $V > V_{mf}$ this figure shows that (P1-P3) increases with gas velocity, while (P1-P2) decreases slightly, stays roughly constant, and increases slightly. This trend is perhaps due to the expansion of the bed and the decrease in the amount of solids between ports 1 and 2. As the gas velocity increases further, the wall shear stress increases and the pressure drop begins to increase.

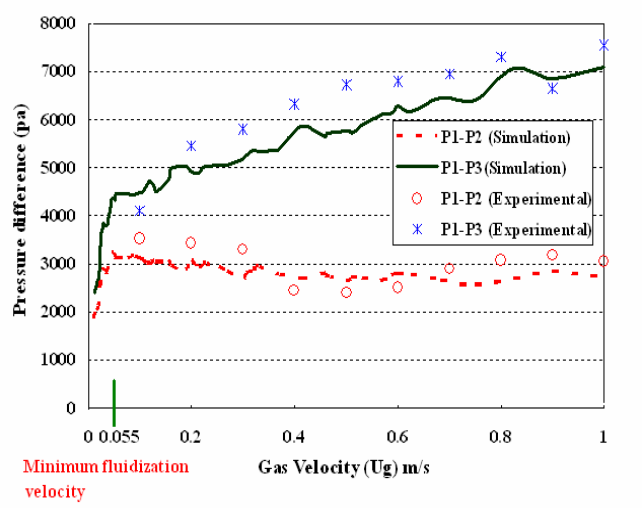
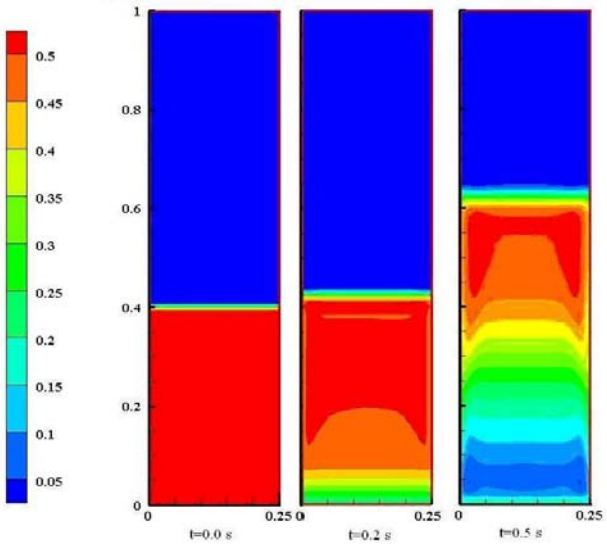


Fig. 2 Comparison of experimental and simulated bed pressure drop versus superficial gas velocity

Figure 3 shows the contour plots of solid fraction in the bed at different times before reaching steady state condition. The bubble formation and the fluctuation pattern of the particles at the surface of the bed are clearly observed from this figure. At time zero, the bed is impulsively fluidized for a superficial gas velocity of V_g=50 cm/s, which is nine times the minimum fluidization velocity V_{mf}. Initially in the time duration of 0 to 1 s, the bed height increases due to bubble formation; in fact, the bed height overshoots the steady-state bed level. The bed height then decreases slightly and levels off to the steady-state bed height after about 2 to 3 s. A careful examination of the simulation results shows that the bubbles at the bottom of the bed are relatively small. The bubbles coalesce as they move upwards producing larger bubbles. The bubbles are also stretched due to the shearing because of interactions with other bubbles and wall effects.

Figure 4 compares the experimental results for bubble formation and bed expansion for different superficial gas velocities. At low gas velocities (lower than Vg=5.5 cm/s), the solids rest on the gas distributor, and the column is in the fixed bed regime. When superficial gas velocity reaches the fluidization velocity of 5.5 cm/s, all particles are entrained by the upward gas flow and the bed is fluidized. At high gas velocities, the movement of solids becomes more vigorous. Such a bed condition is called a bubbling bed or heterogeneous fluidized bed, which corresponds to Vg=20-35 cm/s in Figure 4. In this regime, gas bubbles generated at the distributor coalesce and grow as they rise through the bed. With further increase in the gas velocity (Vg=40-50 cm/s in Figure 4), the intensity of bubble formation and collapse increases sharply.



Open Science Index, Mechanical and Mechatronics Engineering Vol:5, No:6, 2011 publications.waset.org/6657/pdf

Open Science Index, Mechanical and Mechatronics Engineering Vol:5, No:6, 2011 publications.waset.org/6657/pdf

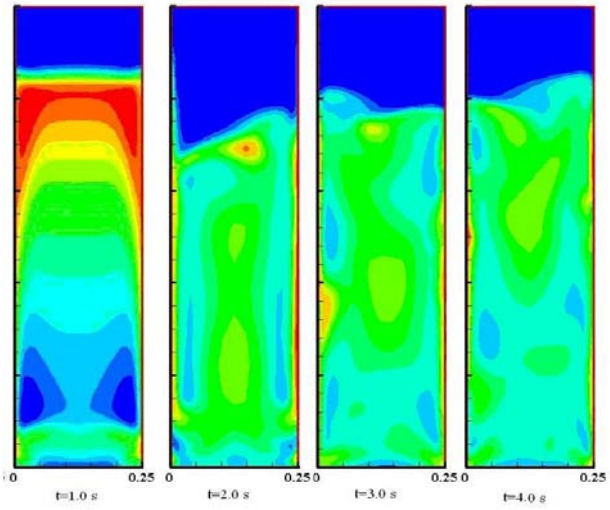


Fig. 3 Simulated solid volume fraction contours in the 2D bed (*Vg* =50 cm/s, drag function: Syamlal–O'Brien)

At higher superficial gas velocities, groups of small bubbles break free from the distributor plate and coalesce, giving rise to small pockets of air. These air pockets travel upward through the particles and burst out at the free surface of the bed, creating the appearance of a boiling bed. Comparison of the contour plots of solid fractions in Figure 3 and the experimental results for bubble formation and bed expansion in Figure 4 for Vg=50 cm/s indicates qualitative similarities of the experimental observations and the simulation results. It should be pointed out that some discrepancies due to the effect of the gas distributor, which was not considered in the CFD model, should be expected. Figure 5 shows the simulation results of gas volume fraction for different superficial gas velocities. Initially, the bed height increases with bubble formation, so gas volume fraction increases and levels off at a steady-state bed height. At the start of the simulation, waves of voidage are created, which travel through the bed and subsequently break to form bubbles as the simulation progresses.

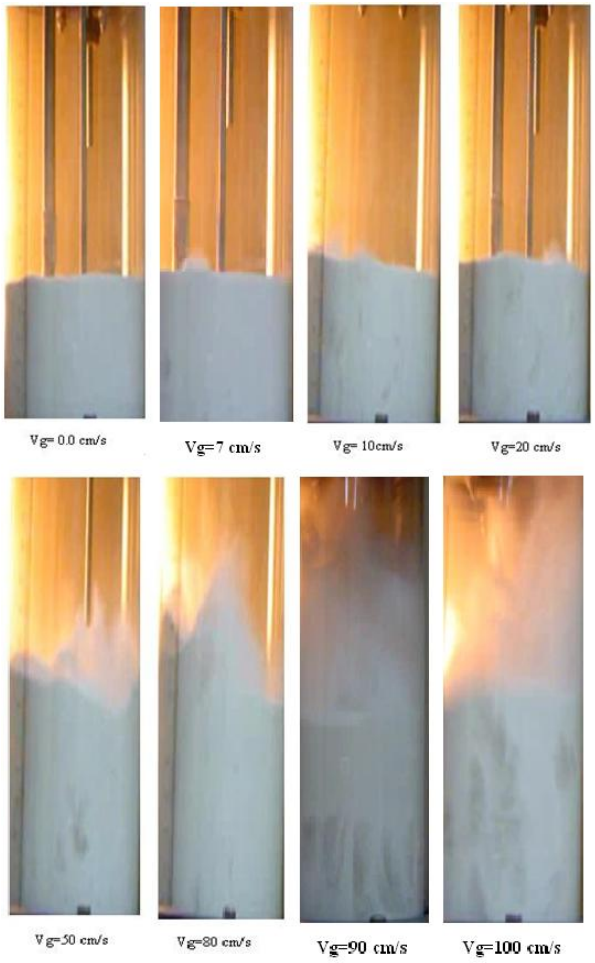


Fig. 4 Comparison of bubble formation and bed expansion for different superficial gas velocities

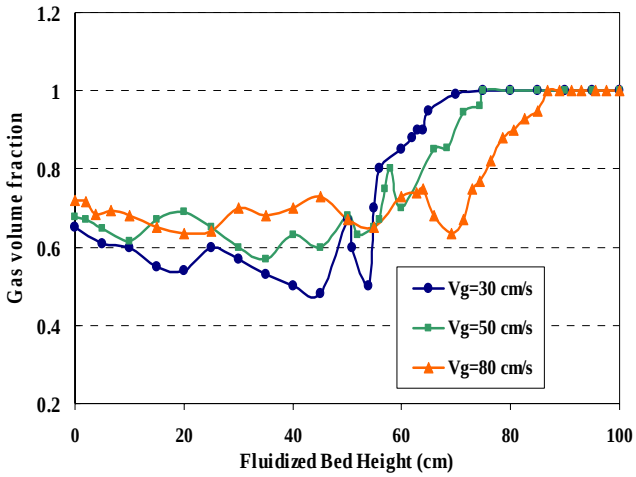


Fig. 5 Simulation results for gas volume fraction at t=5s (Syamlal–O'Brien drag model)

At the bottom of the column, particle concentration is larger than at the upper part. Therefore, the maximum gas volume fraction occurs at the top of the column. Clearly the gas volume fraction of 1 (at the top of the bed) corresponds to the region where the particles are absent. With increasing

Open Science Index, Mechanical and Mechatronics Engineering Vol:5, No:6, 2011 publications.waset.org/6657/pdf

superficial gas velocity, Figure 5 shows that the gas volume fraction generally increases in the bed up to the height of 50 to 60 cm. The gas volume fraction then increases sharply to reach to 1 at the top of the bed. Gas volume fraction approaches the saturation condition of 1 at the bed heights of 63cm, 70cm and 85 cm for Vg=30 cm/s, 50 cm/s and 80 cm/s, respectively.

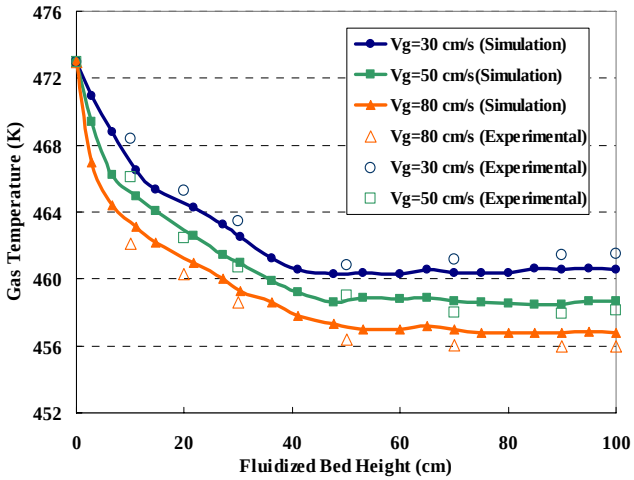


Fig. 6 Simulation and experimental results for inlet gas velocity effect on gas temperature in the bed (t=5 min)

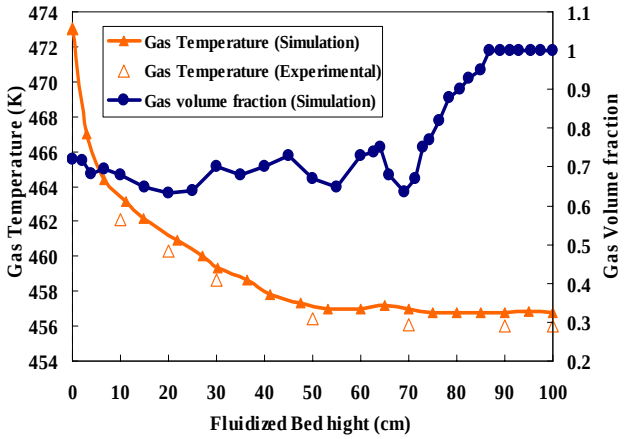


Fig. 7 Comparison of simulation and experimental gas temperature and gas volume fraction at t=5min for Vg=80 cm/s

The influence of inlet gas velocity on the gas temperature is shown in Figures 6 and 7. As noted before, the gas enters the bed with a temperature of 473K, and particles are initially at 300K. Thermocouples are installed along the column as shown in Figure 1. The thermocouple probes can be moved across the reactor for measuring the temperature at different radii. At each height, gas temperatures at five radii in the reactor were measured and averaged. The corresponding gas mean temperatures as function of height are presented in Figures 5 and 7. Figure 6 shows that the gas temperature deceases with height because of the heat transfer between the cold particles and hot gas. Near the bottom of column, solid volume fraction is relatively high; therefore, gas temperature decreases rapidly and the rate of decrease is higher for the region near the bottom of the column. At top of the column, there are no particles (gas volume fraction is one) and the wall is adiabatic; therefore, the gas temperature is roughly constant. Also the results show that with increasing the gas velocity, as expected the gas temperature decreases. From Figures 6 and 9 it is seen that with increasing gas velocity, bed expansion height increases. In addition, the gas temperature reaches to the uniform (constant temperature) condition in the upper region. When gas velocity is 30 cm/s, temperature reaches to its constant value at a height of about 40 cm; and for Vg=50 cm/s and Vg=80 cm/s, the corresponding gas temperatures reaching uniform state, respectively, at heights of 50 and 55 cm. Figure 12 also shows that the simulation results are in good agreement with the experimental data. The small differences seen are the result of the slight heat loss from the wall in the experimental reactor.Figure 7 shows the gas temperature and the gas volume fraction in the same graph. This figure indicates that in the region where the gas volume fraction is highest, the gas temperature is lowest. Clearly in the free gas flow, there is little heat transfer. In the lower part of the reactor, the solid volume fraction is higher, so the rate of heat transfer with the cooler particles is higher and the temperature decreases faster.

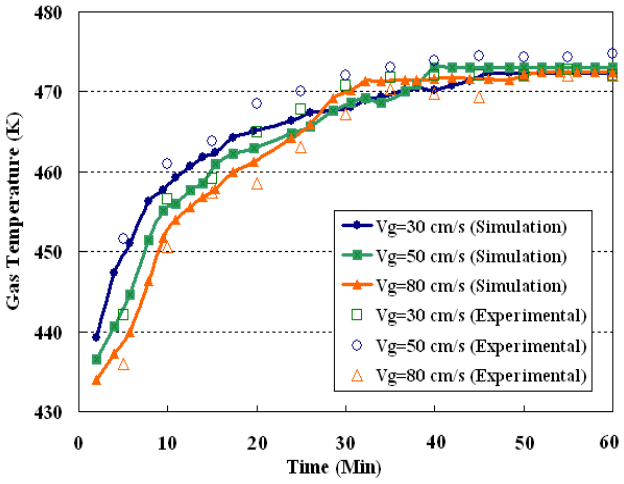


Fig. 8 Comparison of experimental and computational results for gas temperatures at different gas velocities (z=50 cm)

Figure 8 compares the time variation of the simulated gas temperature at z=50 cm for different gas velocities with the experimental data. This figure shows that gas temperature increases with time and the rate of increase varies with somewhat with the gas velocity. The simulation results show that with increasing gas velocity, gas temperature reaches steady state condition rapidly. For Vg=80 cm/s, gas temperature reaches steady state condition after about 30 min; but for Vg=50 and 30 cm/s temperature reaches to steady after 40 and 45min, respectively but there are a few difference between simulation and experimental results.

Open Science Index, Mechanical and Mechatronics Engineering Vol:5, No:6, 2011 publications.waset.org/6657/pdf

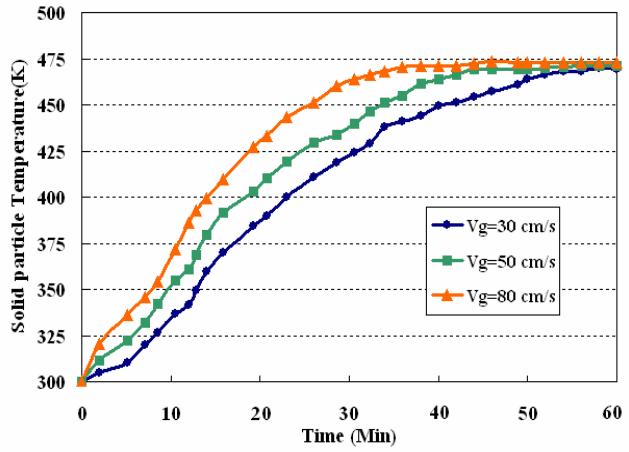


Fig. 9. Simulation results for variation of solid particle temperature with time at different gas velocities at z=50 cm

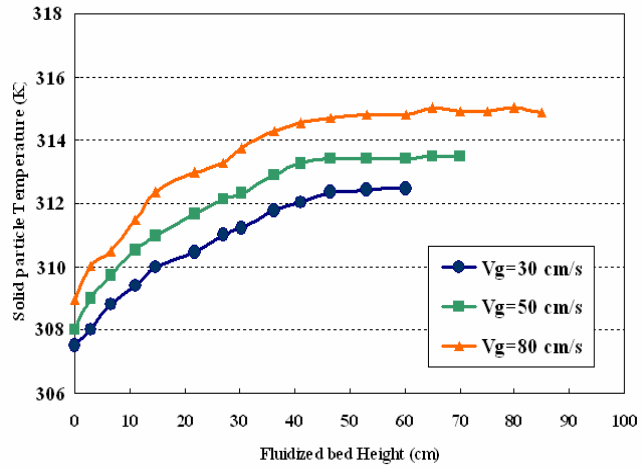


Fig. 10 Inlet gas velocity effect on the simulated solid particle temperatures in bed (t=5min)

For different inlet gas velocities, time variations of the mean solid phase temperature at the height of z=50 cm are shown in Figure 9. The corresponding variation of the averaged solid particle temperature with height is shown in Figure 16. Note that, here, the averaged solid temperature shown is the mean of the particle temperatures averaged across the section of the column at a given height. It is seen that the particle temperature increases with time and with the distance from the bottom of the column. Figure 10 also shows that at higher gas velocity, solid temperature more rapidly reaches the steady state condition. For Vg=80cm/s, solid temperature approaches the steady limit after about 30min; for Vg=50 and 30 cm/s, the steady state condition is reached, respectively, at about 40 and 45min. In addition, initially the temperature differences between solid and gas phases are higher; therefore, the rate of increase of solid temperature is higher. Figure 10 shows that the rate of change of the solid temperature near the bottom of the bed is faster, which is due to a larger heat transfer rate compared to the top of the bed. These figures also indicate that an increase in the gas velocity causes a higher heat transfer coefficient between gas and solid phases, and results in an increase in the solid particle temperature.

V. Conclusions

In this study, unsteady flow and heat transfer in a gas–solid fluidized bed reactor was investigated. The Eulerian-Eulerian model was used for modeling the fluidized bed reactor. The model includes continuity, momentum equations, as well as energy equations for both phases and the equations for granular temperature of the solid particles. A suitable numerical method that employed finite volume method was applied to discritize the governing equations. In order to validate the model, an experimental setup was fabricated and a series of tests were performed. The modeling predictions compared reasonably well with the experimental bed. Pressure drops predicted by the simulations were in relatively close agreement with the experimental measurements. The simulation results suggested that the Syamlal–O'Brien drag model can more realistically predict the hydrodynamics of gas–solid flows for the range of parameters used in this study. Moreover, gas and solid phase temperature distributions in the reactor were computed, considering the hydrodynamics and heat transfer of the fluidized bed. Experimental and numerical results for gas temperature showed that gas temperature decreases as it moves upwards in the reactor. The effects of inlet gas velocity on gas and solid phase temperature was also investigated. The simulation showed that an increase in the gas velocity leads to a decrease in the gas and increase in the solid particle temperatures. Furthermore, comparison between experimental and computational simulation showed that the model can predict the hydrodynamic and heat transfer behavior of a gas-solid fluidized bed reasonably well.

References

[1] Gidaspow, D., Multiphase Flow and Fluidization, First ed. Academic press, London, 1994.
[2] Kunii, D., Levenspiel ,O., Fluidization Engineering, Second ed. Butterworth-Heinemann, Boston, 1991.
[3] Ranade, V.V., Computational Flow Modeling for Chemical Reactor Engineering, First ed, New York, 2002.
[4] Grace, J.R., Taghipour, F., Verification and validation of CFD models and dynamic similarity for fluidized beds. Powder Technology , 139, 99–110, 2004.
[5] Bird, R.B., Stewart, W.E., Lightfoot, E.N., Transport Phenomena. seconded . Wiley, New York, 2002.
[6] Taghipour, F., Ellis, N., Wong, C., Experimental and computational study of gas–solid fluidized bed hydrodynamics, Chemical Engineering Science, 60, 6857–6867, 2005.
[7] Kaneko Y., Shiojima, T., Horio, M., DEM simulation of fluidized beds for gas-phase olefin polymerization, Chemical Engineering Science, 54, 5809–5821, 1999.
[8] Rong. F., Marchisio. D.L., Fox. R.O., CFD Simulation of Polydisperse Fluidized-Bed Polymerization Reactors, Department of Chemical Engineering, Iowa State University, 2114 Sweeney Hall, Ames, IA 50010-2230, USA, Preprint submitted to Elsevier Science, August 2003.
[9] Gobin, H. Neau, O. Simonin, J. Llinas, V. Reiling, J.L. Selo, Fluid dynamic numerical simulation of a gas phase polymerization reactor, International Journal for Numerical Methods in Fluids, 43,1199–1220, 2003.
[10] Van Wachem, B.G.M., Schouten, J.C., Van den Bleek, C.M., Krishna, R., Sinclair, J.L., Comparative analysis of CFD models of dense gas–solid systems, AIChE Journal, 47, 1035–1051, 2001.

[11] Van Wachem, B.G.M., Schouten, J.C., Van den Bleek, C.M., Krishna, R., Sinclair, J.L., CFD modeling of gas-fluidized beds with a bimodal particle mixture, AIChE Journal, 47, 1292–1302, 2001.
[12] Chiesa, M., Mathiesen, V., Melheim, J.A.., Halvorsen, B., Numerical simulation of particulate flow by the Eulerian–Lagrangian and the Eulerian–Eulerian approach with application to a fluidized bed, Computers & Chemical Engineering, 29, 291–304, 2005.
[13] Syamlal, M., O'Brien, T.J., Computer simulation of bubbles in a fluidized bed. A.I.Ch.E., 85, 22–31,1989.
[14] Syamlal, M., O'Brien, T.J., Fluid dynamic simulation of O3 decomposition in a bubbling fluidized bed. A.I.Ch.E. Journal 49, 2793–2801, 2003
[15] Huilin, L., Yurong, H., Gidaspow, D., Hydrodynamic modeling of binary mixture in a gas bubbling fluidized bed using the kinetic theory of granular flow, Chemical Engineering Science, 58, 1197–1205, 2003.
[16] Lun, C.K.K., and Savage, S.B., A Simple Kinetic Theory for Granular Flow of Rough, Inelastic, Spherical Particles, J. Appl. Mech., 54, 47-53, 1987.
[17] Zhong.W, Zhang.M, Jin.B, Zhang.Y, Xiao.R, Huang.Y, Experimental investigation of particle mixing behavior in a large spout-fluid bed, Chemical Engineering and Processing, 2007.
[18] Patankar, S.V., Numerical heat transfer and fluid flow, First ed. Hemisphere Publishing, Washington, DC, 1980.
[19] Gidaspow, D., Hydrodynamics of Fluidization and Heat Transfer: Supercomputer Modeling, Appl. Mech. Rev., 39, 1986.
[20] Hamzehei, M., Rahimzadeh, H., Experimental and Numerical Study of Hydrodynamics with Heat Transfer in a Gas-Solid Fluidized bed Reactor at Different Particle Sizes, Ind. Eng. Chem. Res., 48, 3177–3186, 2009.
[21] Hamzehei, M., Rahimzadeh, H., Ahmadi, G., Computational and Experimental Study of Heat Transfer and Hydrodynamics in a 2D Gas-Solid Fluidized Bed Reactor, Ind. Eng. Chem. Res., (Special Issue) 49, pp. 5110–5121, 2010.
[22] Hamzehei, M., Rahimzadeh, H., Ahmadi, G., Studies of gas velocity and particles size effects on fluidized bed hydrodynamics with CFD modeling and experimental investigation, Journal of Mechanics, 26, pp. 113-124, 2010.
[23] Hamzehei, M. and Rahimzadeh, H., "Investigation of a Fluidized Bed Chamber Hydrodynamics with Heat Transfer Numerically and Experimentally," Korean Journal of Chemical Engineering, 27, pp. 355.363, 2010.

Open Science Index, Mechanical and Mechatronics Engineering Vol:5, No:6, 2011 publications.waset.org/6657/pdf